Electronic Supplementary Material (ESI) for Materials Chemistry Frontiers.

Supporting information

A Stable Pyridone-Based Hydrogen-Bonded Organic Framework for Electrochemical Detection of Dopamine

Yong-Min Liu, [a,b] Bai-Tong Liu, *[c] Yu-Lin Li, [a,b] Jin-Lin Li, [a,d] Tian-Fu Liu[a,b] and Lei Cai*[a]

[a] State Key Laboratory of Structural Chemistry, Fujian Institute of Research on the Structure of Matter, Chinese Academy of Sciences, Fuzhou, Fujian 350002, P. R. China
[b] University of Chinese Academy of Sciences, Beijing, 100049, P. R. China
[c] Department of Chemistry, The University of Hong Kong, Pokfulam Road, Hong Kong SAR 999077, P.R. China
[d] College of Chemistry and Materials Science, Fujian Normal University, Fuzhou 350007, P. R. China
Email: baitong@hku.hk; tfliu@fjirsm.ac.cn; cailei@fjirsm.ac.cn

Content:

Experimental section

1. General information

1.1 Materials

Unless otherwise noted, all reagents and solvents including tetrakis(triphenylphosphine)palladium ($Pd(PPh_3)_4$), chlorotrimethylsilane (TMSCl), potassium carbonate (K_2CO_3), potassium iodide (KI), methanol (MeOH), ethanol (EtOH), dimethyl sulfoxide (DMSO), *N,N*-Dimethylformamide (DMF), ethyl acetate (EA), toluene, acetonitrile (MeCN), acetone, tetrahydrofuran (THF), trifluoroacetic acid (TFA), 1,4-dioxane, cyclohexane and dichloromethane (CH_2Cl_2) were sourced from commercial suppliers and used as received without additional purification. For electrochemical studies, deionized water obtained from the Millipore Milli-Q system (resistivity 18.2 MΩ cm) was employed.

1.2 Characterizations

We conducted the following analyses and measurements using the specified equipment:

1. Nuclear Magnetic Resonance (NMR): ^{1}H-NMR and ^{13}C-NMR spectra were recorded on a Bruker AVANCE III spectrometer at 400 MHz and 151 MHz, respectively.
2. Single Crystal X-ray Diffraction: Single crystal X-ray diffraction data was collected on a Bruker D8 VENTURE diffractometer equipped with Cu-Kα radiation (λ=1.5418 Å).
3. Calculation of Theoretical Free Volume: The PLATON program (1.8 Å probe radius) was used to calculate the theoretical free volume of guest molecules in **PFC-65**.
4. Powder X-ray Diffraction (PXRD): PXRD patterns were collected on a Rigaku Smartlab X-ray diffraction instrument.
5. Thermo-Gravimetric Analysis (TGA): TGA was performed on a NETZSCH STA 449F3 instrument. The samples were heated at a rate of 5°C/min from 50 to 800°C under N_2 atmosphere.
6. CO_2 Gas Adsorption Isotherms: Adsorption isotherms at 195 K and 298 K for CO_2 gas were measured on an ASAP 2020 micromeritics surface characterization analyzer. Activation of **PFC-65** was performed under vacuum condition (0.2 kPa) in 10 h at 120°C to remove guest solvents for adsorption experiments.
7. Water Vapor Adsorption Isotherm: Water vapor adsorption isotherm was measured on a Micromeritics 3Flex Surface Characterization Analyzer at room temperature.
8. Ultraviolet and Visible (UV–vis) Absorption Spectra: Solid UV–vis absorption spectra were collected at room temperature on a Shimadzu UV–2550 spectrophotometer equipped with Lab sphere integrating, using $BaSO_4$ as standards.
9. Photoluminescence (PL) Spectra: PL spectra were acquired on an Edinburgh FS5 spectrometer equipped with a continuous xenon lamp under a 380-nm excitation.
10. Infrared (IR) Spectra: IR spectra were collected by a VERTEX70 series FT–IR

spectrometer.

2. Monomer synthesis

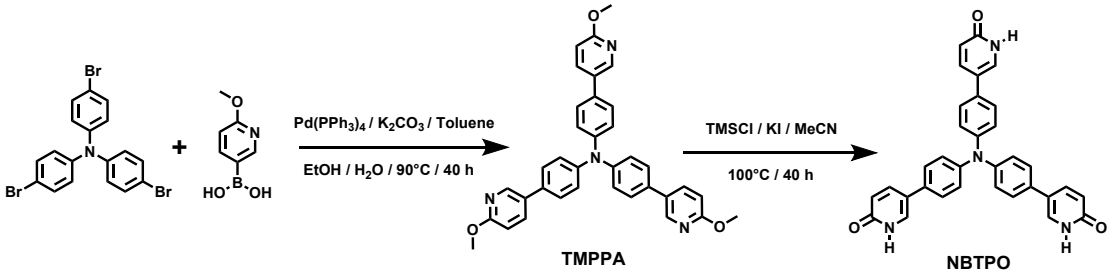

Scheme S1. The synthetic route of NBTPO

2.1 Synthesis of tris(4-(6-methoxypyridin-3-yl) phenyl) amine (TMPPA)

A mixture solution of toluene/ethanol/deionized water (25/15/15 mL) was added to a double-necked round-bottom flask. After adequate removal of oxygen by bubbling nitrogen into the flask, tris (4-bromophenyl) amine (2.41 g, 5 mmol), (6-methoxypyridin-yl) boronic acid (3.294 g, 15 mmol), $Pd(PPh_3)_4$ (346.7 mg, 0.3 mmol), and K_2CO_3 (2.764 g, 20 mmol) were added into the solution, before stirring and refluxing at 90°C under N_2 atmosphere for 40 h. The reaction was cooled to room temperature after the starting materials completely consumed, which was detected by thin-layer chromatograph (TLC). The volatile toluene and ethanol were removed by rotary evaporation. Then, the reaction mixture was extracted with ethyl acetate (20 mL, ×3). The combined organic phases filtered through a short pad of neutral Al_2O_3 (200 mesh) to remove insoluble solid, such as Pd species. The filtrate was concentrated by rotary evaporation. The residue was dissolved in acetone and further purified by recrystallization with the evaporation of acetone. The desired tris(4-(6-methoxypyridin-3-yl) phenyl) amine was obtained (2.6 g, 4.6 mmol, yield: 92%) as colorless powder after drying in the oven overnight.

2.2 Synthesis of 5,5',5''-(nitrilotris (benzene- 4,1-diyl)) tris(pyridin-2(1*H*)-one) (NBTPO)

Tris(4-(6-methoxypyridin-3-yl) phenyl) amine (2.32 g, 4.1 mmol) and KI (2.04 g, 12.3 mmol) were added into a 250 mL oven-dried flask charged with 100 mL acetonitrile and a stirring bar under N_2 atmosphere. Subsequently, trimethylchlorosilane (TMSCl, 1.56 mL, 12.3 mmol) was injected into the flask with a syringe and stirred at 100°C for 40 h. After cooling to room temperature, the compound was obtained by centrifugation and washed by water (*NOTE*: saturated Na_2SO_3 solution was added to reduce the iodine produced in the reaction mixture), and washed by ethanol and ethyl acetate for three times to remove organic impurities. The resultant white solids (1.83 g, 3.49 mmol) were obtained with a yield of 85%. ^{1}H-NMR (400 MHz, DMSO-d_6): δ (ppm) = 11.83 (s, 3H), 7.77 (d, J = 4.0 Hz, 3H), 7.63 (s, 3H), 7.46 (d, J = 4.0 Hz, 6H), 7.00 (d, J = 4.0 Hz, 6H), 6.37 (d, J = 4.0 Hz, 3H). ^{13}C-NMR (151 MHz, TFA-d_4): δ (ppm) = 160.69, 150.48, 149.27, 134.94, 134.60, 129.99, 129.57,

127.05, 116.42.

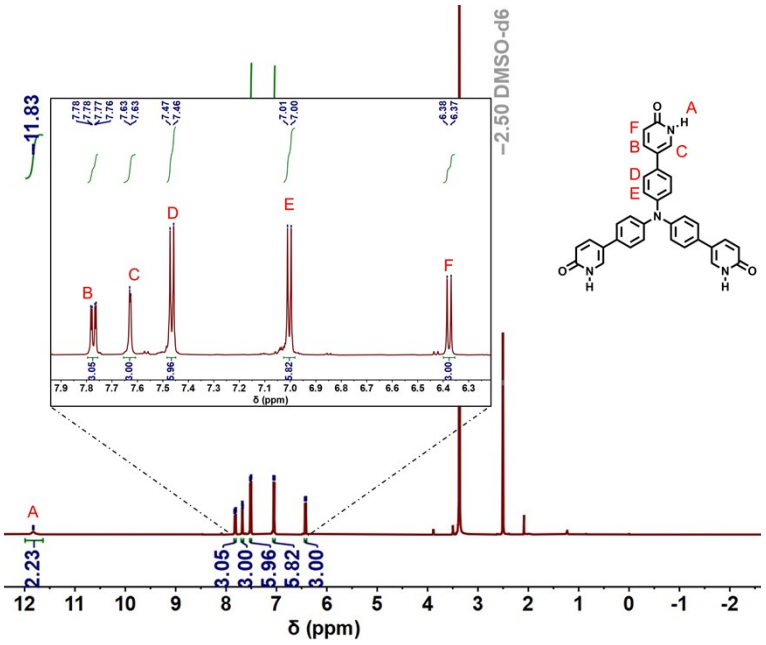

Fig. S1 ^{1}H-NMR spectrum of NBTPO

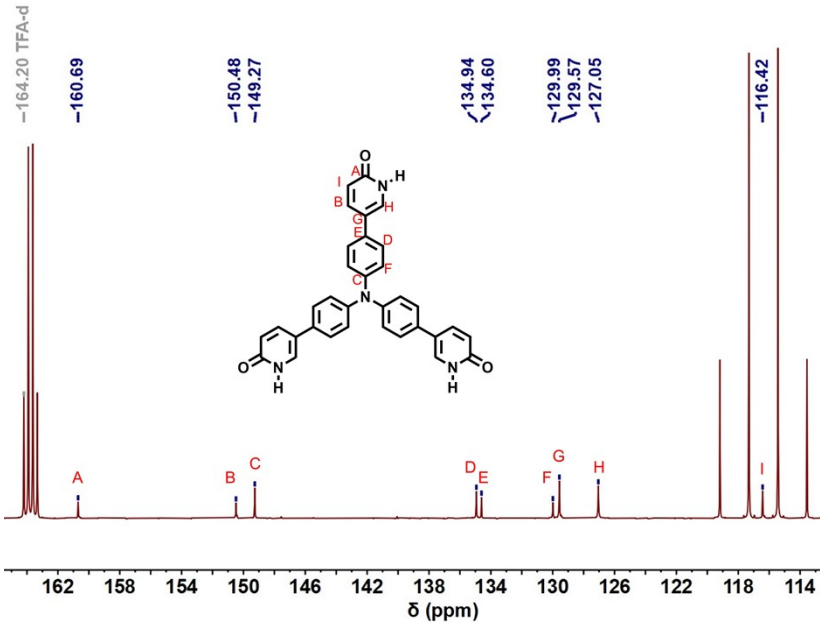

Fig. S2 ^{13}C-NMR spectrum of NBTPO

3. Preparation of PFC-65, PFC-65a and nanoPFC-65a

NBTPO (4 mg, 0.0076 mmol) was dissolved in 1 mL DMSO at 100°C in a 10-mL vial. Then the opened vial was put in a bigger glass container (with lid) contained with methanol. The colorless and transparent flaky crystals, named as PFC-65, were obtained by slow vapor diffusion for three days in a 45°C oven. The size of PFC-65 was about 0.25×0.12×0.005 mm^3. After removal of the mother liquid, the guest DMSO in the crystals was exchanged with methanol for 15 times. The solvent-exchanged samples were activated by vacuum at 80°C under a pressure of 0.2 kPa for 10 h, and

PFC-65a crystals were obtained.

nanoPFC-65a is synthesized by ball-milling NBTPO (100 mg) with 50 μL acetone at 20 Hz for 15 min and activated as described above.

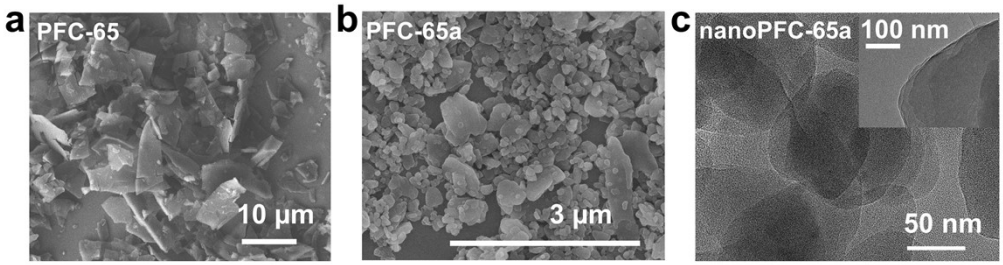

Fig. S3 SEM images of (a) PFC-65 and (b) PFC-65a; (c) TEM images of nanoPFC-65a

4. Preparation of nPFC-65a/GCE and electrochemical measurements

The glassy carbon electrode (GCE) with a diameter of 3.0 mm, underwent polishing step using alumina powders and washed with ethanol and water. To prepare the nanoPFC-65a coating solution, NanoPFC-65a was uniformly dispersed in ethanol solution contained 5% (v/v%) Nafion through ultrasonication. 10-μL portion of the stock solution was then dropwise coated on a clean glassy carbon electrode and left to dry at room temperature.

For the electrochemical measurements, phosphate buffer solutions (PBS) (0.1 M) with a concentration of 0.1 M and varying pH levels were prepared. In the experimental setup, A GCE served as the working electrode, a platinum mesh electrode was used as the counter electrode, and an Ag/AgCl electrode (saturated KCl, aq) was employed as the reference electrode.

The potential range of cyclic voltammetry (CV) measurements were set from −0.2 V to 0.6 V in different scan rates. To obtain well-defined oxidation current peaks for DA detection, the differential pulsed voltammetry (DPV) measurements were performed within a potential ranged from 0 to 0.6 V. The parameters for DPV were configured with an amplitude of 50 mV, a pulse width of 0.5 s, and a pulse period of 1 s. Different concentrations of DA were prepared by diluting a high-concentration DA solution.

5. Characterization

5.1 PFC-65 structure information

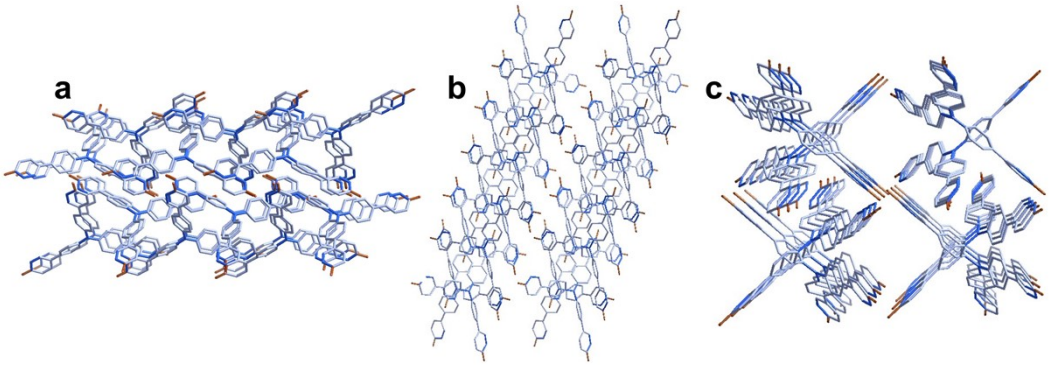

Fig. S4 Crystal structure of PFC-65 viewed from (a) *a*-axis; (b) *b*-axis and *c*-axis

Table S1 Crystal structure data of PFC-65

Identification code	PFC-65
CCDC number	2292651
Empirical formula	$C_{33}H_{24}N_4O_3$
Formula weight	524.56
Temperature (K)	293(2)
Crystal system	monoclinic
Space group	$P2_1/c$
a (Å)	13.9675(18)
b (Å)	18.9635(14)
c (Å)	12.3056(10)
α (°)	90
β (°)	109.706(11)
γ (°)	90
Volume (Å^3)	3068.5(6)
Z	4
ρ_{calc} (g/cm^3)	1.135
μ (mm^{-1})	0.598
F(000)	1096.0
Crystal size (mm^3)	0.3×0.2×0.005
Radiation	Cu Kα
2θ range for data collection (°)	6.722 to 156.046
Reflections collected	20175
Independent reflections	6232 (R_{int} = 0.0440, R_{sigma} = 0.0396)
Data/restraints/parameters	6232/0/361
Goodness-of-fit on F^2	1.064
Final R indexes [I≥2σ(I)]	R_1 = 0.0784, wR_2 = 0.2402
Final R indexes [all data]	R_1 = 0.1020, wR_2 = 0.2683
Largest diff. peak and hole (e/Å^3)	0.73/-0.33
Completeness	99.8%

5.2 Powder X-ray diffraction patterns

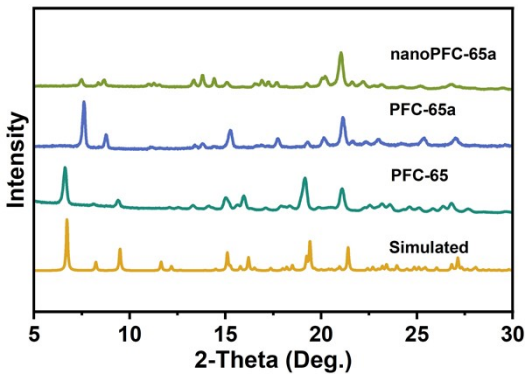

Fig. S5 The PXRD patterns of simulated, as-synthesized PFC-65, PFC-65a and nanoPFC-65a

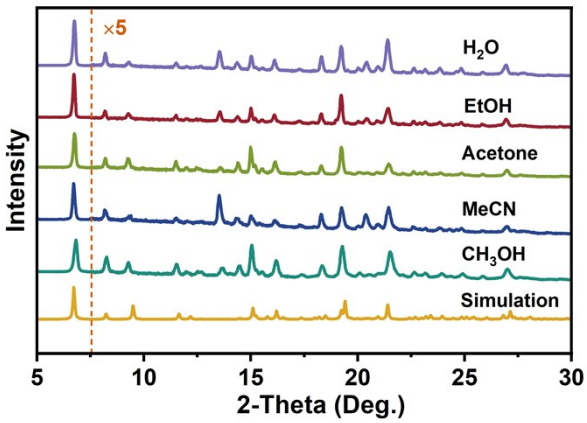

Fig. S6 PXRD patterns of PFC-65 from various solvents diffusion, '×5' in the figure means that the data after the dividing line is magnified five times.

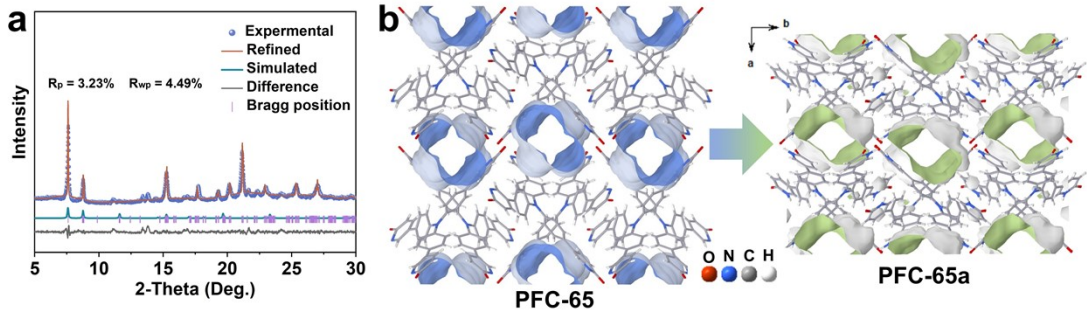

Fig. S7 (a) PXRD patterns and Pawley refinement of PFC-65a; (b) Schematic diagram of PFC-65 transformed into PFC-65a viewed from the *c*-axis

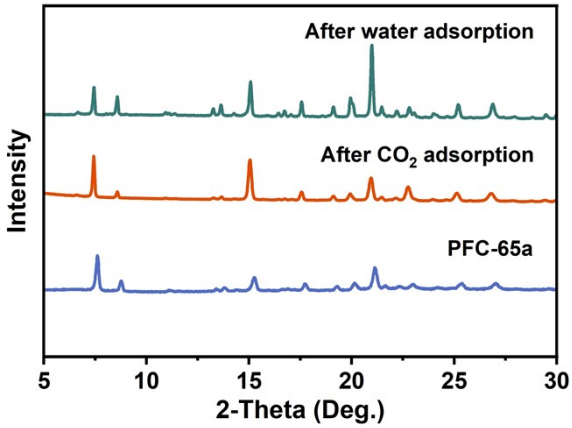

Fig. S8 PXRD patterns of PFC-65a after water vapor and CO_2 adsorption

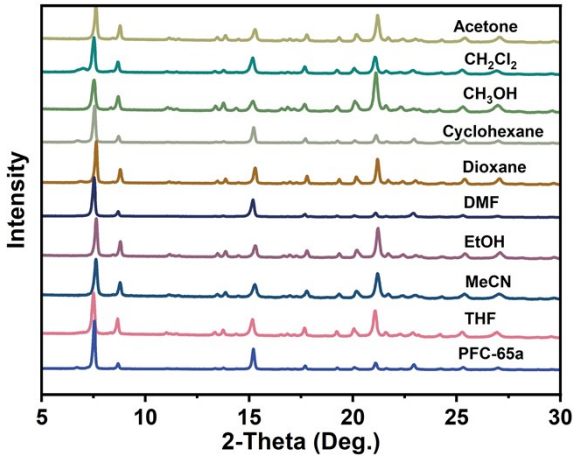

Fig. S9 PXRD patterns of PFC-65a after being treated with different organic solvents

5.3 Fourier transform infrared spectroscopy (FT–IR)

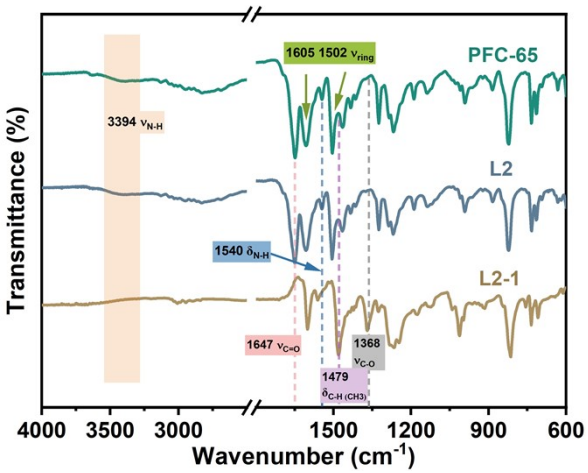

Fig. S10 FT–IR spectra of PFC-65, NBTPO and TMPPA

5.4 UV-vis and PL spectra

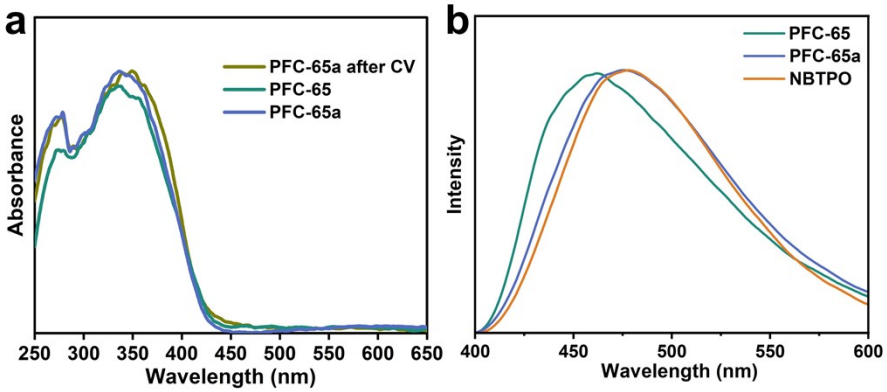

Fig. S11 (a) UV-vis absorption spectra and (b) PL spectra of PFC-65, PFC-65a and amorphous monomers

5.5 Thermogravimetric analyses of PFC-65 and PFC-65a

TGA curves showed PFC-65 had a significant weight loss before 200°C, because of the guest of solvents (CH_3OH and DMSO). It was almost disappeared in the activated PFC-65. PFC-65 can maintain stable before 400°C.

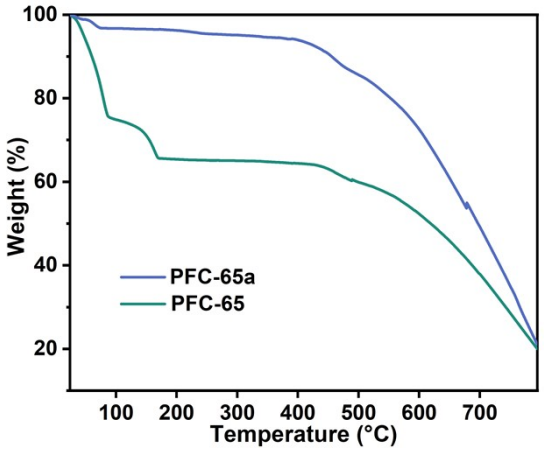

Fig. S12 TGA curves of as-synthesized PFC-65 and PFC-65a

5.6 Water contact angle experiment at 20°C

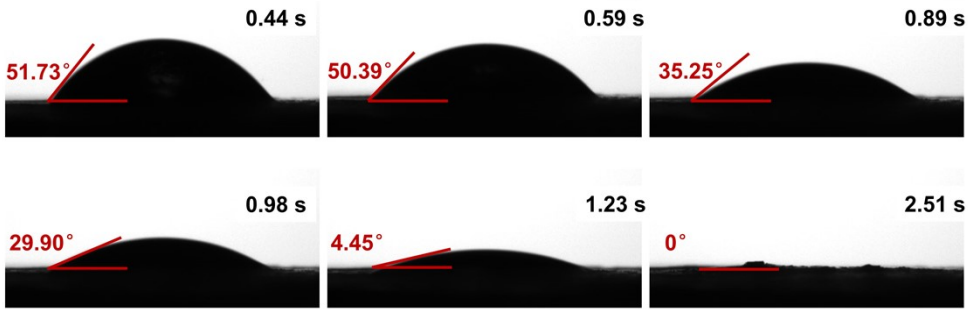

Fig. S13 The water contact angles of PFC-65a

5.7 Electrochemical data

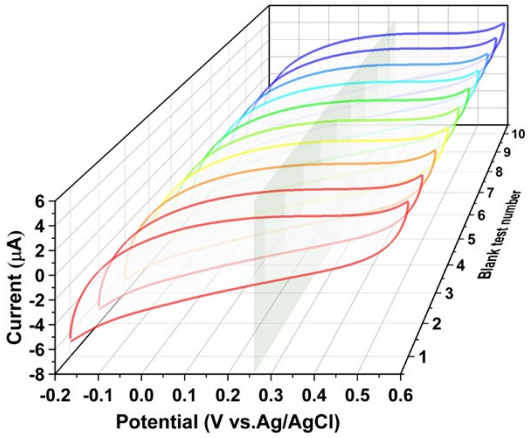

Fig. S14 CV curves of ten blank tests (without DA) on nPFC-65a/GCE using a 0.1 M phosphate-buffered saline (PBS) electrolyte at pH 7

The oxidation current responses at potential of 0.26 V were collected and listed on Table S2 to calculate the standard deviation of blank tests.

Table S2 Current values of blank test at 0.26 V

Number	1	2	3	4	5	6	7	8	9	10	RSD
Current	3.509	3.479	3.521	3.53	3.473	3.479	3.484	3.49	3.495	3.498	0.01898

Table S3 Analytical performance comparison of previously reported works and this work

Material	Method	Sensitivity ($\mu A\ mM^{-1}$)	Linear range (μM)	LOD (μM)
[1]V_2O_5@PANI	CA	15	6.6-110	39
[2]RGO-ZnO	DPV	328	1-70	0.33
[3]Graphene/ZIF-8	CA	340	3-1000	1
[4]Cu(tpa)-GO composite	DPV	774.2	1-50	0.21
[5]MIL-101/GO	SWV	-	1-10 and 10-100	1
[6]HKUST-1/ERGO	DPV	155.3	0.2-300	0.013
[7]Graphene/Nafion	DPV	2672	0.5-35	0.33
[8]MOF-525–PEDOT NTs composite	DPV	30	2-270	0.04
nPFC-65a/GCE	DPV	17	4-400	3.499

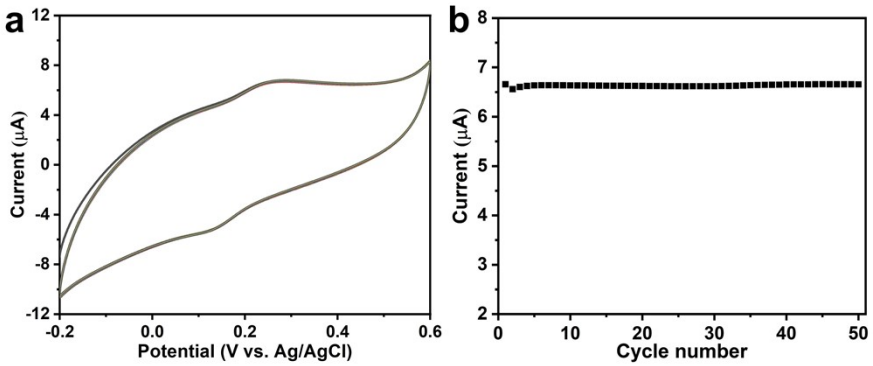

Fig. S15 The cyclicity stability of nPFC-65a/GCE. (a) 50 circles of CV curves detection of 50-μM DA; (b) The oxidation peak current of 50 circles of CV curves using a 0.1 M phosphate-buffered saline (PBS) electrolyte at pH 7

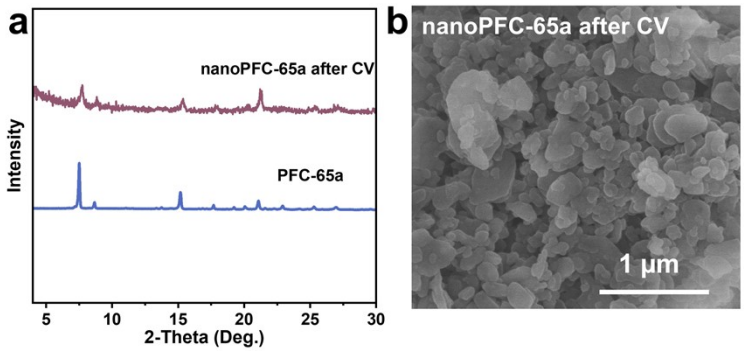

Fig. S16 (a) PXRD patterns and (b) SEM image of nanoPFC-65a after CV sensing

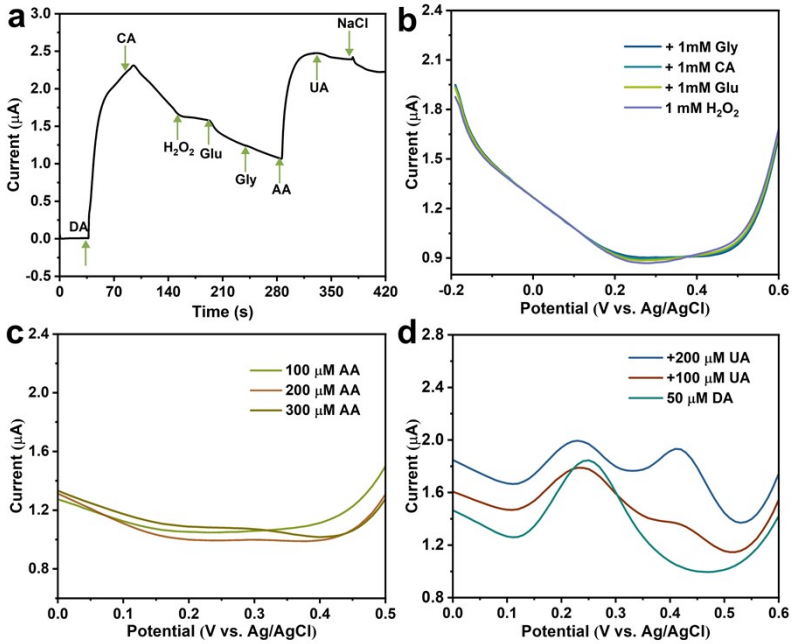

Fig. S17 (a) Amperometric response of dopamine (DA), citric acid (CA), H_2O_2, glucose (Glu), glycine (Gly), ascorbic acid (AA), uric acid (UA) and NaCl on nPFC-65a/GCE at 0.26 V under constant stirring (DA:100 μM, interferences: 1 mM, 0.1 M PBS, pH=7); nPFC-65a/GCE was used for the DPV detection of (b) CA, H_2O_2, Glu, and Gly; (c) different concentrations of AA; (d) different concentrations of UA with 50-μM DA in PBS

Table S4 The Zeta potential of DA and nanoPFC-65a in water

Sample	Mean Zeta potential (mV)
DA	+4.2
PFC-65a	–30.35

References

1 R. Suresh, K. Giribabu, R. Manigandan, S. P. Kumar, S. Munusamy, S. Muthamizh and V. Narayanan, Characterization and dopamine sensing property of V_2O_5@polyailine nanohybrid, *Synth. Met.*, 2014, **196**, 151-157.

2 X. Zhang, Y. C. Zhang and L. X. Ma, One-pot facile fabrication of graphene-zinc oxide

composite and its enhanced sensitivity for simultaneous electrochemical detection of ascorbic acid, dopamine and uric acid, *Sens. Actuators B Chem.*, 2016, **227**, 488-496.

3 Y. Y. Zheng, C. X. Li, X. T. Ding, Q. Yang, Y. M. Qi, H. M. Zhang and L. T. Qu, Detection of dopamine at graphene-ZIF-8 nanocomposite modified electrode, *Chin. Chem. Lett.*, 2017, **28**, 1473-1478.

4 X. Wang, Q. Wang, Q. Wang, F. Gao, F. Gao, Y. Yang and H. Guo, Highly dispersible and stable copper terephthalate metal-organic framework-graphene oxide nanocomposite for an electrochemical sensing application, *ACS Appl. Mater. Interfaces*, 2014, **6**, 11573-11580.

5 J. H. Yang, D. Yang and Y. Li, Graphene supported chromium carbide material synthesized from Cr-based MOF/graphene oxide composites, *Mater. Lett.*, 2014, **130**, 111-114.

6 B. Ma, H. Guo, M. Wang, L. Li, X. Jia, H. Chen, R. Xue and W. Yang, Electrocatalysis of Cu-MOF/graphene composite and its sensing application for electrochemical simultaneous determination of dopamine and paracetamol, *Electroanalysis*, 2019, **31**, 1002-1008.

7 D. Kim, S. Lee and Y. Piao, Electrochemical determination of dopamine and acetaminophen using activated graphene-nafion modified glassy carbon electrode, *J. Electroanal. Chem.*, 2017, **794**, 221-228.

8 T. Y. Huang, C. W. Kung, Y. T. Liao, S. Y. Kao, M. Cheng, T. H. Chang, J. Henzie, H. R. Alamri, Z. A. Alothman, Y. Yamauchi, K. C. Ho and K. C. W. Wu, Enhanced charge collection in MOF-525-PEDOT nanotube composites enable highly sensitive biosensing, *Adv. Sci.*, 2017, **4**, 1700261.